of the autocorrelation scans also consistently shows an amplitude enhancement by more than 20% when the phase lock is activated.

An important issue will be to demonstrate control over the phase profile across the entire synthesized spectrum, namely pulse shaping. For example, a flat spectral phase profile is a prerequisite for generating an ultrashort pulse while arbitrary shape is needed for coherent control applications. Using the current control scheme, the carrier-envelope slip phases of the two lasers track each other ($\Delta\phi_1 = \Delta\phi_2$). There remains, of course, a static phase difference between the two lasers, namely ($\phi_1 - \phi_2$). However, this static phase can be controlled through an appropriate phase offset introduced in the carrier heterodyne beat detection, for example, through phase shift of the radio frequency signal driving the AOM. This phase-compensated spectrum can then be used in a pulse-shaping device to generate the desired pulse waveform.

References and Notes

1. M. H. Anderson, J. R. Ensher, M. R. Matthews, C. E. Wieman, E. A. Cornell, *Science* **269**, 198 (1995).
2. C. A. Sackett *et al.*, *Nature* **404**, 256 (2000).
3. R. S. Judson, H. Rabitz, *Phys. Rev. Lett.* **68**, 1500 (1992).
4. D. E. Spence, P. N. Kean, W. Sibbett, *Opt. Lett.* **16**, 42 (1991).
5. J. P. Zhou *et al.*, *Opt. Lett.* **19**, 1149 (1994).
6. R. Ell *et al.*, *Opt. Lett.* **26**, 373 (2001).
7. R. R. Alfano, *The Supercontinuum Laser Source* (Springer-Verlag, New York, 1989).
8. J. K. Ranka, R. S. Windeler, A. J. Stentz, *Opt. Lett.* **25**, 25 (2000).
9. P. B. Corkum, N. H. Burnett, M. Y. Ivanov, *Opt. Lett.* **19**, 1870 (1994).
10. A. E. Kaplan, *Phys. Rev. Lett.* **73**, 1243 (1994); A. V. Sokolov, D. R. Walker, D. D. Yavuz, G. Y. Yin, S. E. Harris, *Phys. Rev. Lett.* **85**, 562 (2000).
11. R. A. Kaindl *et al.*, *J. Opt. Soc. Am. B* **17**, 2086 (2000).
12. R. W. Schoenlein *et al.*, *Science* **274**, 236 (1996).
13. R. L. Byer, *J. Mod. Opt.*, in press.
14. J. Ye, J. L. Hall, *Opt. Lett.* **24**, 1838 (1999).
15. T. Udem, J. Reichert, R. Holzwarth, T. W. Hänsch, *Opt. Lett.* **24**, 881 (1999).
16. _____, *Phys. Rev. Lett.* **82**, 3568 (1999).
17. S. A. Diddams *et al.*, *Phys. Rev. Lett.* **84**, 5102 (2000).
18. J. Ye, J. L. Hall, S. A. Diddams, *Opt. Lett.* **25**, 1675 (2000).
19. L. Hollberg *et al.*, *IEEE J. Quantum Electron.*, in press.
20. D. J. Jones *et al.*, *Science* **288**, 635 (2000).
21. A. Apolonski *et al.*, *Phys. Rev. Lett.* **85**, 740 (2000).
22. H. R. Telle *et al.*, *Appl. Phys. B* **69**, 327 (1999).
23. Supplemental material is available at *Science* Online at www.sciencemag.org/cgi/content/full/293/5533/1286/DC1
24. M. T. Asaki *et al.*, *Opt. Lett.* **18**, 977 (1993).
25. L. S. Ma, R. K. Shelton, H. Kapteyn, M. Murnane, J. Ye, *Phys. Rev. A*, **64**, 021802(R) (2001).
26. S. A. Crooker, F. D. Betz, J. Levy, D. D. Awschalom, *Rev. Sci. Instrum.* **67**, 2068 (1996).
27. D. W. Allan, *Proc. IEEE* **54**, 221 (1966).
28. D. N. Fittinghoff *et al.*, *Opt. Lett.* **21**, 884 (1996).
29. J.-C. Diels, W. Rudolph, *Ultrashort Laser Pulse Phenomena: Fundamentals, Techniques, and Applications on a Femtosecond Time Scale* (Academic Press, San Diego, CA, 1996).

30. We are indebted to D. Anderson for the loan of essential equipment and S. T. Cundiff for critical comments. We also thank R. Bartels, T. Weinacht, and S. Backus for useful discussions. The work at JILA is supported by NIST, NASA, NSF, and the Research Corporation.

19 April 2001; accepted 4 July 2001

Nanowire Nanosensors for Highly Sensitive and Selective Detection of Biological and Chemical Species

Yi Cui,[1]* Qingqiao Wei,[1]* Hongkun Park,[1] Charles M. Lieber[1,2]†

Boron-doped silicon nanowires (SiNWs) were used to create highly sensitive, real-time electrically based sensors for biological and chemical species. Amine- and oxide-functionalized SiNWs exhibit pH-dependent conductance that was linear over a large dynamic range and could be understood in terms of the change in surface charge during protonation and deprotonation. Biotin-modified SiNWs were used to detect streptavidin down to at least a picomolar concentration range. In addition, antigen-functionalized SiNWs show reversible antibody binding and concentration-dependent detection in real time. Lastly, detection of the reversible binding of the metabolic indicator Ca^{2+} was demonstrated. The small size and capability of these semiconductor nanowires for sensitive, label-free, real-time detection of a wide range of chemical and biological species could be exploited in array-based screening and in vivo diagnostics.

Planar semiconductors can serve as the basis for chemical and biological sensors in which detection can be monitored electrically and/or optically (*1*–*4*). For example, a planar field effect transistor (FET) can be configured as a sensor by modifying the gate oxide (without gate electrode) with molecular receptors or a selective membrane for the analyte of interest; binding of a charged species then results in depletion or accumulation of carriers within the transistor structure (*1*, *2*). An attractive feature of such chemically sensitive FETs is that binding can be monitored by a direct change in conductance or related electrical property, although the sensitivity and potential for integration are limited.

The physical properties limiting sensor devices fabricated in planar semiconductors can be readily overcome by exploiting nanoscale FETs (*5*–*9*). First, binding to the surface of a nanowire (NW) or nanotube (NT) can lead to depletion or accumulation of carriers in the "bulk" of the nanometer diameter structure (versus only the surface region of a planar device) and increase sensitivity to the point that single-molecule detection is possible. Second, the small size of NW and NT building blocks and recent advances in assembly (*9*, *10*) suggest that dense arrays of sensors could be prepared. Indeed, NT FETs were shown recently by Dai and co-workers to function as gas sensors (*11*). Calculations suggested that direct binding of electron-withdrawing NO_2 or electron-donating NH_3 gas molecules to the NT surface chemically gated these devices. However, several properties of NTs could also limit their development as nanosensors, including the following: (i) existing synthetic methods produce mixtures of metallic and semiconducting NTs, which make systematic studies difficult because metallic "devices" will not function as expected, and (ii) flexible methods for the modification of NT surfaces, which are required to prepare interfaces selective for binding a wide range of analytes, are not well established.

Nanowires of semiconductors such as Si do not have these limitations, as they are always semiconducting, and the dopant type and concentration can be controlled (*7*–*9*), which enables the sensitivity to be tuned in the absence of an external gate. In addition, it should be possible to exploit the massive knowledge that exists for the chemical modification of oxide surfaces, for example, from studies of silica (*12*) and planar chemical and biological sensors (*4*, *13*), to create semiconductor NWs modified with receptors for many applications. Here we demonstrate the potential of NW nanosensors with direct, highly sensitive real-time detection of chemical and biological species in aqueous solution.

The underlying concept of our experiments is illustrated first for the case of a pH nanosensor (Fig. 1A). Here a silicon NW (SiNW) solid state FET, whose conductance is modulated by an applied gate, is transformed into a nanosensor by modifying the silicon oxide surface with 3-aminopropyltriethoxysilane (APTES) to provide a surface

[1]Department of Chemistry and Chemical Biology, Harvard University, Cambridge, MA 02138, USA. [2]Division of Engineering and Applied Sciences, Harvard University, Cambridge, MA 02138 USA.

*These authors contributed equally to the work.
†To whom correspondence should be addressed. E-mail: cml@cmliris.harvard.edu

that can undergo protonation and deprotonation, where changes in the surface charge can chemically gate the SiNW. The single-crystal boron-doped (p-type) SiNWs used in these studies were prepared by a nanocluster-mediated vapor-liquid-solid growth method described previously (*7*, *8*, *14*). Devices were fashioned by flow aligning (*10*) SiNWs on oxidized silicon substrates and then making electrical contacts to the NW ends with electron-beam lithography (*7*, *8*, *15*). Linear current (*I*) versus voltage (*V*) behavior was observed for all of the devices studied, which shows that the SiNW-metal contacts are ohmic, and applied gate voltages produced reproducible and predictable (*7*, *8*) changes in the *I-V*. In the solid state FET (insets, Fig. 1B), the conductance (dI/dV) measured in air at $V = 0$ as a function of time (*15*) was stable for a given gate voltage and showed a stepwise increase with discrete changes of the gate voltage from 10 to –10 V; plots of conductance versus gate voltage were nearly linear.

The response of the conductance of APTES-modified SiNWs (*16*) to changes in solution pH was evaluated by fabricating a cell consisting of a microfluidic channel formed between a poly(dimethylsiloxane) (PDMS) mold (*10*, *17*) and the SiNW/substrate. We could carry out continuous flow or static experiments and could readily change pH. Measurements of conductance as a function of time and solution pH (Fig. 1B) demonstrate that the NW conductance increases stepwise with discrete changes in pH from 2 to 9 and that the conductance is constant for a given pH; the changes in conductance are also reversible for increasing and/or decreasing pH. A typical plot of the conductance versus pH (Fig. 1C) shows that this pH dependence is linear over the pH 2 to 9 range and thus suggests that modified SiNWs could function as nanoscale pH sensors. In addition, we believe the uncertainty in slope of the conductance versus pH obtained from the different SiNW pH sensors studied to date, 100 ± 20 nS/pH, is quite good and could be improved by placing further effort on controlling reproducibility of the SiNW surface modification.

These results can be understood by considering the mixed surface functionality of the modified SiNWs. Covalently linking APTES to SiNW oxide surface results in a surface terminating in both $-NH_2$ and $-SiOH$ groups (Fig. 1A), which have different dissociation constants, pK_a (*12*, *18*, *19*). At low pH, the $-NH_2$ group is protonated to $-NH_3^+$ (*18*) and acts as a positive gate, which depletes hole carriers in the p-type SiNW and decreases the conductance. At high pH, $-SiOH$ is deprotonated to $-SiO^-$, which correspondingly causes an increase in conductance. The observed linear response can be attributed to an approximately linear change in the total surface charge density (versus pH) because of the combined acid and base behavior of both surface groups. To support this point, we also carried out pH-dependent measurements on unmodified (only $-SiOH$ functionality) SiNWs (Fig. 1D). These conductance measurements show a nonlinear pH dependence: The conductance change is small at low pH (2 to 6) but large at high pH range (6 to 9). Notably, these pH measurements on unmodified SiNWs are in excellent agreement with previous measurements of the pH-dependent surface charge density derived from silica (*19*) (Fig. 1D).

To explore biomolecular sensors, we functionalized SiNWs with biotin (*20*) and studied the well-characterized ligand-receptor binding of biotin-streptavidin (Fig. 2A) (*21*). Measurements show that the conductance of biotin-modified SiNWs increases rapidly to a constant value upon addition of a 250 nM streptavidin solution and that this conductance value is maintained after the addition of pure buffer solution (Fig. 2B). The increase in conductance upon addition of streptavidin is consistent with binding of a negatively charged species to the p-type SiNW surface and the fact that streptavidin ($pI \sim 5$ to 6) (*21*) is negatively charged at the pH of our measurements. The absence of a conductance decrease with addition of pure buffer is also consistent with the small dissociation constant ($K_d \sim 10^{-15}$ M) and correspondingly small dissociation rate for biotin-streptavidin (*21*).

In addition, several control experiments were carried out to confirm that the observed conductance changes are due to the specific binding of streptavidin to the biotin ligand. First, addition of a streptavidin solution to an unmodified SiNW did not produce a change

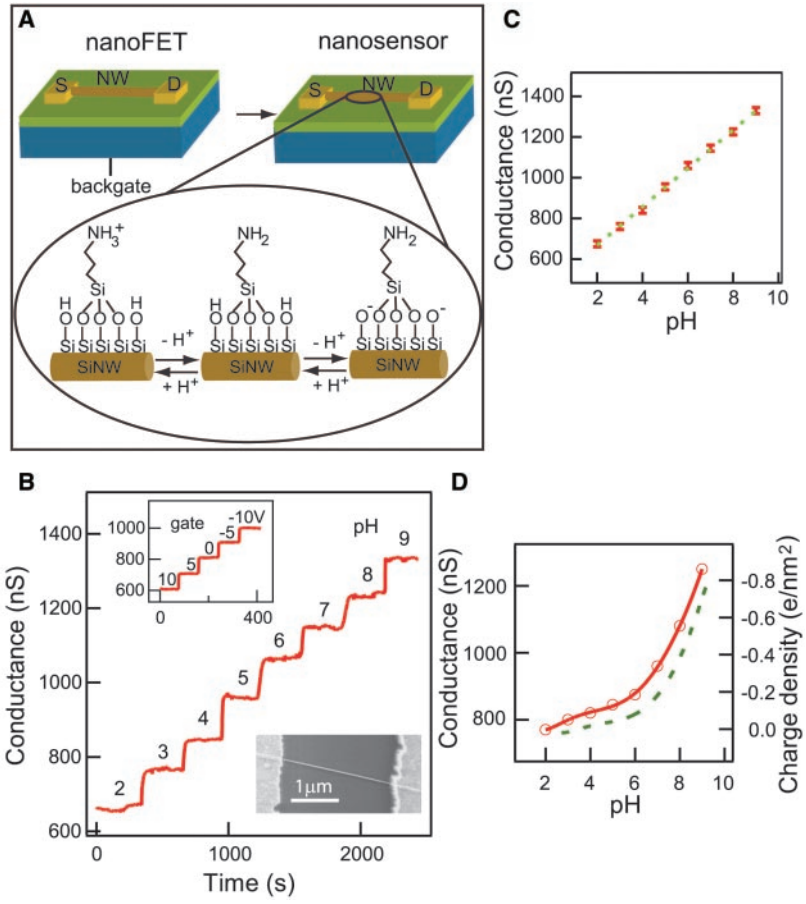

Fig. 1. NW nanosensor for pH detection. (**A**) Schematic illustrating the conversion of a NW FET into NW nanosensors for pH sensing. The NW is contacted with two electrodes, a source (S) and drain (D), for measuring conductance. Zoom of the APTES-modified SiNW surface illustrating changes in the surface charge state with pH. (**B**) Real-time detection of the conductance for an APTES-modified SiNW for pHs from 2 to 9; the pH values are indicated on the conductance plot. (inset, top) Plot of the time-dependent conductance of a SiNW FET as a function of the back-gate voltage. (inset, bottom) Field-emission scanning electron microscopy image of a typical SiNW device. (**C**) Plot of the conductance versus pH; the red points (error bars equal ± 1 SD) are experimental data, and the dashed green line is linear fit through this data. (**D**) The conductance of unmodified SiNW (red) versus pH. The dashed green curve is a plot of the surface charge density for silica as a function of pH. [Adapted from (*19*)]

in conductance (Fig. 2C). Second, addition of a streptavidin solution in which the biotin-binding sites were blocked by reaction with 4 equivalents of d-biotin produced essentially no change in the conductance of biotin-modified SiNWs (Fig. 2D). These controls show that there is little nonspecific binding of the protein to either bare or biotin-modified SiNW surfaces.

We also explored the sensitivity limits of biotin-modified SiNWs nanosensors and find that it is possible to detect streptavidin binding down to a concentration of at least 10 pM (Fig. 2E) (*22*). This detection level is substantially lower than the nanomolar range demonstrated recently by stochastic sensing of single molecules (*23*). In addition, a time-dependent increase in the conductance can be resolved immediately after streptavidin addition at very low concentrations. We believe that this behavior reflects contributions from the forward binding rate and/or diffusion, although future studies will be required to resolve these contributions.

The above studies demonstrate that our NW nanosensors are capable of highly sensitive and selective real-time detection of proteins, although the essentially irreversible biotin-streptavidin binding interaction precludes real-time monitoring of varying protein concentrations. To explore this issue, we studied the reversible binding of monoclonal antibiotin (m-antibiotin) with biotin (*24*). Time-dependent conductance measurements made on biotin-modified SiNWs (Fig. 3A) exhibit a well-defined drop after addition of m-antibiotin solution (*20*) followed by an increase in the conductance to about the original value upon addition of pure buffer solution. The time scale for the increase in conductance (seconds), which we associate with m-antibiotin dissociation, is consistent with the reported (*24*) dissociation rate constant, $\sim 0.1\ s^{-1}$, for this antibody-antigen system. The decrease in conductance upon m-antibiotin addition indicates that a positively charged species binds to and gates the SiNW and is also consistent with the positive charge of m-antibiotin at the pH 7 of our experiments (*25*, *26*). Control experiments demonstrate that the observed results are due to specific antibody binding to the surface antigen. First, unmodified SiNWs do not exhibit a conductance change after adding m-antibiotin (Fig. 3B). Second, addition of immunoglobulin G (IgG), which is not specific for biotin, does not result in a change in conductance, whereas subsequent addition of m-antibiotin solution produces a conductance drop, as observed in Fig. 3C.

We extended these reversible, real-time antibody detection experiments by monitoring the SiNW sensor conductance as a function of m-antibiotin concentration. We observed a linear change in the conductance as a function of m-antibiotin concentration below ~10 nM and saturation at higher values (Fig. 3D). There are several important facts that can be gleaned from this data. First, from the linear regime, we estimate that the dissociation constant, K_d, is on the order of 10^{-9} M, which is in good agreement with the value, $\sim 10^{-9}$ M, determined previously (*25*). Second, we can monitor protein concentration in real time, which could have important implications in basic research, for example, monitoring protein expression, and medical diagnostics. Lastly, preliminary experiments suggest that the linear response dynamic range can be extended by applying a back gate to the nanowire, where gating can either increase or decrease the intrinsic binding constant.

The concept of using NW FETs modified with receptors or ligands for specific detection can also be extended in many directions. As a final example, we investigated sensing of calcium ions (Ca^{2+}), which are important for activating biological processes such as muscle contraction, protein secretion, cell death, and development (*27*). We created a Ca^{2+} sensor by immobilizing calmodulin onto SiNW surfaces. Data recorded from modified SiNW devices (Fig. 4A) showed a drop in the conductance upon addition of a 25 μM Ca^{2+} solution and a subsequent increase

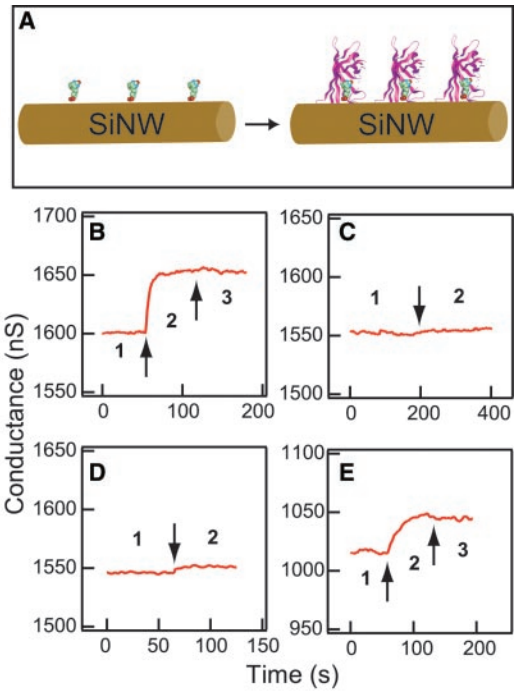

Fig. 2. Real-time detection of protein binding. (**A**) Schematic illustrating a biotin-modified SiNW (left) and subsequent binding of streptavidin to the SiNW surface (right). The SiNW and streptavidin are drawn approximately to scale. (**B**) Plot of conductance versus time for a biotin-modified SiNW, where region 1 corresponds to buffer solution, region 2 corresponds to the addition of 250 nM streptavidin, and region 3 corresponds to pure buffer solution. (**C**) Conductance versus time for an unmodified SiNW; regions 1 and 2 are the same as in (B). (**D**) Conductance versus time for a biotin-modified SiNW, where region 1 corresponds to buffer solution and region 2 to the addition of a 250 nM streptavidin solution that was preincubated with 4 equivalents d-biotin. (**E**) Conductance versus time for a biotin-modified SiNW, where region 1 corresponds to buffer solution, region 2 corresponds to the addition of 25 pM streptavidin, and region 3 corresponds to pure buffer solution. Arrows mark the points when solutions were changed.

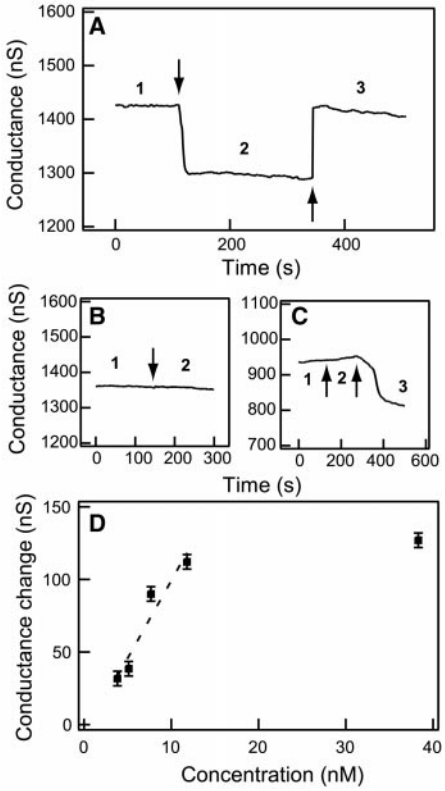

Fig. 3. Real-time detection of reversible protein binding. (**A**) Plot of conductance versus time for a biotin-modified SiNW, where region 1 corresponds to buffer solution, region 2 corresponds to the addition of ~3 μM m-antibiotin (460 μg/ml), and region 3 corresponds to flow of pure buffer solution. (**B**) Conductance versus time for an unmodified SiNW; regions 1 and 2 are the same as in (A). (**C**) Conductance versus time for a biotin-modified SiNW, where region 1 corresponds to buffer solution, region 2 corresponds to the addition of bovine IgG (200 μg/ml), and region 3 corresponds to addition of ~3 μM m-antibiotin (460 μg/ml). Arrows mark the points when the solutions were changed. (**D**) Plot of the conductance change of a biotin-modified SiNW versus m-antibiotin concentration; the dashed line is a linear fit to the four low concentration data points. Error bars equal ± 1SD.

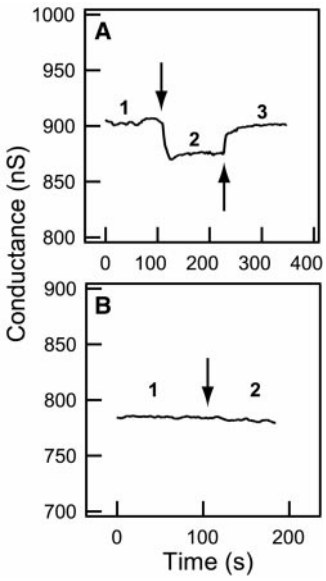

Fig. 4. Real-time detection of Ca^{2+} ions. (**A**) Plot of conductance versus time for a calmodulin-terminated SiNW, where region 1 corresponds to buffer solution, region 2 corresponds to the addition of 25 μM Ca^{2+} solution, and region 3 corresponds to pure buffer solution. (**B**) Conductance versus time for an unmodified SiNW; regions 1 and 2 are the same as in (A). Arrows mark the points when solutions were changed. Calmodulin-modified NWs were prepared by placing a drop (~20 μl) of calmodulin solution (250 μg/ml) on SiNW for 1 hour and then rinsing with water for three times.

when a Ca^{2+}-free buffer was subsequently flowed through the device. Control experiments carried out with unmodified SiNWs (Fig. 4B) did not exhibit a conductance change when Ca^{2+} is added and thus demonstrate that the calmodulin receptor is essential for detection. In addition, the observed conductance decrease in modified SiNWs is consistent with expected chemical gating by positive Ca^{2+}, and the estimated dissociation constant, 10^{-5} to 10^{-6} M, is consistent with the reported K_d for calmodulin (*27*).

References and Notes

1. P. Bergveld, *IEEE Trans. Biomed. Eng.* **BME-19**, 342 (1972).
2. G. F. Blackburn, in *Biosensors: Fundamentals and Applications*, A. P. F. Turner, I. Karube, G. S. Wilson, Eds. (Oxford Univ. Press, Oxford, 1987), pp. 481–530.
3. D. G. Hafeman, J. W. Parce, H. M. McConnell, *Science* **240**, 1182 (1988).
4. F. Seker, K. Meeker, T. F. Kuech, A. B. Ellis, *Chem. Rev.* **100**, 2505 (2000).
5. S. J. Tans, A. R. M. Verschueren, C. Dekker, *Nature* **393**, 49 (1999).
6. P. G. Collins, M. S. Arnold, P. Avouris, *Science* **292**, 706 (2001).
7. Y. Cui, X. Duan, J. Hu, C. M. Lieber, *J. Phys. Chem. B* **104**, 5213 (2000).
8. Y. Cui, C. M. Lieber, *Science* **291**, 851 (2001).
9. X. Duan, Y. Huang, Y. Cui, J. Wang, C. M. Lieber, *Nature* **409**, 66 (2001).
10. Y. Huang, X. Duan, Q. Wei, C. M. Lieber, *Science* **291**, 891 (2001).
11. J. Kong *et al.*, *Science* **287**, 622 (2000).
12. R. K. Iler, *The Chemistry of Silica* (Wiley, New York, 1979).
13. P. N. Bartlett, in *Handbook of Chemical and Biological Sensors*, R. F. Taylor, J. S. Schultz, Eds. (IOP Publishing, Philadelphia, 1996), pp. 139–170.
14. Y. Cui, L. J. Lauhon, M. S. Gudiksen, J. Wang, C. M. Lieber, *Appl. Phys. Lett.* **78**, 2214 (2001).
15. SiNWs with diameters of either 10 or 20 nm were suspended in ethanol and flow aligned on oxidized Si substrates (1 to 10 ohm·cm, 600-nm oxide; Silicon Sense), and contact leads (50 nm Al or Ti + 100 nm Au) were defined with electron-beam lithography. The separation between contacts was typically 2 to 4 μm. The conductance of SiNW devices as a function of time was determined directly with a computerized apparatus with lock-in amplifier (Stanford Research, SR 830); a 31-Hz sine wave with 30-mV amplitude at zero dc bias was used in most measurements. The conductances of the SiNW devices were between 500 and 2000 nS (resistance, 2 megohms to 500 kilohms). This relatively small range testifies to the good control of doping in our NWs.
16. Surface-functionalized SiNW devices were prepared by cleaning in an oxygen plasma (0.35 torr, 25 W power for 20 s) to remove contaminants, immersion in 1% ethanol solution of APTES (Aldrich) for 20 min, rinsing with ethanol for three times, followed by heating at 120°C for 5 min. The different pH solutions were made from 10 mM phosphate buffers with 100 mM NaCl. Solutions were flowed through PDMS microchannels (*10*, *17*) (100- to 200-μm width and height) at a flow rate of 0.5 ml/hour. The parasitic conductance through the solution was a constant (about 10 nS) and less than the signal from the SiNW (about 100 nS).
17. D. C. Duffy, J. C. McDonald, O. J. A. Schueller, G. M. Whitesides, *Anal. Chem.* **70**, 4974 (1998).
18. D. V. Vezenov, A. Noy, L. F. Rozsnyai, C. M. Lieber, *J. Am. Chem. Soc.* **119**, 2006 (1997).
19. G. H. Bolt, *J. Phys. Chem.* **61**, 1166 (1957).
20. Biotin-modified SiNWs were prepared by depositing a drop (~20 μl) of phosphate-buffered solution (PBS) (250 μg/ml; pH 5.6) solution of biotinamidocaproyl-labeled bovine serum albumin (Sigma) on SiNWs for 2 hours, followed by a five times rinse with buffer solution. The solutions used to probe biotin-streptavidin binding were 1 mM phosphate buffer (pH 9) with 10 mM NaCl. The d-biotin–saturated streptavidin solution was prepared by adding four equivalents of d-biotin (Sigma) to one equivalent of streptavidin. All the solutions used in biotin and m-antibiotin (Sigma) binding studies were 1 mM phosphate buffer (pH 7) with 5 mM NaCl. The parasitic conductance in these experiments, ≤5 nS, was substantially less than the sensor signal, 40 to 100 nS.
21. M. Wilchek, E. A. Bayer, *Methods Enzymol.* **184**, 49 (1990).
22. In addition, the detection sensitivity can be changed by the doping concentration and should enable single-molecule detection at sufficiently low concentration. As an example, a single charge on the NW surface will be detected if it generates a sufficiently large local potential barrier (>100 meV at room temperature) for electronic motion. Assuming that a single charge is ~1 nm away from a 20-nm-diameter NW, the carrier concentration will most likely be lower than the order of ~1000 electrons/μm (or a few electrons/nm) for detection, which translates into 3×10^{18} to 10^{19} cm^{-3}.
23. L. Movileanu, S. Howorka, O. Braha, H. Bayley, *Nature Biotechnol.* **18**, 109 (2000).
24. R. C. Blake II, A. R. Pavlov, D. A. Blake, *Anal. Biochem.* **272**, 123 (1999).
25. H. Bagci, F. Kohen, U. Kuscuoglu, E. A. Bayer, M. Wilchek, *FEBS Lett.* **322**, 47 (1993).
26. Sequence analysis shows that the binding region of antibiotin (IgG1) is positively charged at pH 7 (*24*). The remaining domains of this large protein are relatively distant from the SiNW and thus should have little effect on SiNW conductance.
27. C. B. Klee, T. C. Vanaman, *Adv. Protein Chem.* **35**, 213 (1982).

28. We thank L. Lauhon, L. Chen, and Q. Cui for helpful discussion and T. Deng for technical assistance. C.M.L. acknowledges support of this work by the Office of Naval Research and the Defense Advanced Projects Research Agency.

21 May 2001; accepted 23 July 2001

Stable Ordering in Langmuir-Blodgett Films

Dawn Y. Takamoto,[1] Eray Aydil,[1] Joseph A. Zasadzinski,[1]* Ani T. Ivanova,[2] Daniel K. Schwartz,[2]† Tinglu Yang,[3] Paul S. Cremer[3]

Defects in the layering of Langmuir-Blodgett (LB) films can be eliminated by depositing from the appropriate monolayer phase at the air-water interface. LB films deposited from the hexagonal phase of cadmium arachidate (CdA_2) at pH 7 spontaneously transform into the bulk soap structure, a centrosymmetric bilayer with an orthorhombic herringbone packing. A large wavelength folding mechanism accelerates the conversion between the two structures, leading to a disruption of the desired layering. At pH > 8.5, though it is more difficult to draw LB films, almost perfect layering is obtained due to the inability to convert from the as-deposited structure to the equilibrium one.

Langmuir-Blodgett films are made by pulling a substrate through a monolayer of amphiphilic molecules at the air-water interface. Under the appropriate conditions, the monolayer is transferred to the substrate (*1*, *2*). Although the LB technique has been used for decades, applications of the method have been frustrated by defects ranging from pinholes to larger scale reorganization of the layers (Fig. 1A) (*3*, *4*). We show here that this reorganization is the progression from the as-deposited structure to the thermodynamic equilibrium structure. However, as Fig. 1B shows, the reorganization can be slowed to the point that nearly perfect LB multilayer films can be made by depositing from a different monolayer phase that exists at the air-water interface at pH > 8.5. The high-pH monolayer phase has a more condensed and lower energy lattice structure than the monolayer at pH